JOURNAL OF APPLIED ELECTROCHEMISTRY 11 (1981) 751–763

Fundamentals of lead-acid cells. XVII. The a.c. impedance of lead dioxide formed in sulphuric acid on some lead alloys

N. A. HAMPSON, S. KELLY
Department of Chemistry, University of Technology, Loughborough, Leicestershire, LE11 3TU, UK

K. PETERS
Chloride Technical Ltd, Wynne Avenue, Swinton, Manchester M27 2HB, UK

Received 16 February 1981

The impedances of PbO_2 formed on lead and some lead alloys have been measured over a wide range of potential. Conditions were chosen so that well-defined electrode states were obtained. Considerable differences were observed in the behaviour of alloys containing antimony and bismuth. The latter alloying ingredient appears to contribute some semiconducting properties to lead sulphate films formed on PbO_2 by polarizing them at potentials negative to the reversible potential in sulphuric acid.

Nomenclature

C_L	double-layer capacitance
C_X	series capacitance
D	diffusion coefficient
E	potential
R_{CT}	charge-transfer resistance
R_Ω	electrolyte resistance
Z_D	impedance as defined by Equation 1
Z_F	impedance as defined by Equation 2
Z'	impedance as defined by Equation 3
σ	Warburg coefficient
ω	angular frequency

1. Introduction

The impedance method for measuring the rates of electrochemical reactions and hence investigating their kinetics is a very powerful technique [1]. Some studies have been made of the lead dioxide electrode. The impedance of massive β-PbO_2 films electrodeposited on Pt have been investigated [2, 3] and compared with those from simple porous films produced by electro-oxidation in sulphuric acid of basic lead sulphate pasted on to lead. It was found possible to obtain some useful kinetic data from the massive β-PbO_2 system. The appearance of a high-frequency semicircle in the Sluyters plots observed over a wide range of potential enables the charge transfer resistance to be estimated. A plot of $\log R_{CT}$ versus E enabled the charge transfer coefficient to be calculated as 0.3, and the exchange current density of 2.4×10^{-5} A cm^{-2} was shown to be quite reasonable for the electrode in 5 M H_2SO_4 at 1044 mV†. A further interesting feature of these measurements was that the surface of a freshly plated electrode was found to be continuously changing with time. A plot showed this change to result in the charge transfer resistance increasing logarithmically with time. It was argued that this resulted from the progressive thickening of a lead sulphate layer nucleated upon the massive lead dioxide. When the layer is sufficiently thick the diameter of the high-frequency semicircle becomes very large and the electrode ultimately becomes insulated from the electrolyte solution. The frequency response of the porous lead dioxide electrode was quite complex and showed an interesting high-frequency region which included an inductive loop. The presence of this inductive loop had also been observed by Keddam *et al.* [4] who studied the lead–acid cell at various stages of discharge. Keddam suggested that geometrical effects were the cause of the inductive loops whereas it seemed to us that the occurrence of the reaction over a

† All potentials are referred to the Hg/Hg_2SO_4 (s) electrode in the same solution.

0021–891X/81/060751–13$03.30/0

distributed region of the electrode as discussed by Darby [5] provided a more realistic explanation.

As the electrode is driven to more negative potentials the Sluyters plot curves over towards the real axis reaching the limit of $\pi/8$ to the real axis. This is what is to be expected for an electrode with semi-infinite pores at right angles to the front of the electrode. This line ultimately degenerates into a more complex shape; at these potentials (700 mV), however, the electrode is largely transformed to lead sulphate. In this region the impedance spectrum was very complicated and discussion of the shapes obtained in the far lead sulphate region were very difficult to interpret. It was decided to attempt to simplify the complex Sluyters plots obtained from the very complex porous (0.05 cm thick) electrode by first investigating the impedance of lead dioxide/lead sulphate films on the base electrode. Current industrial practice uses lead dioxide on a lead–antimony or lead–calcium–tin alloy for the majority of applications of the lead–acid cell, although there is minor interest in the Planté situation where the lead dioxide films are developed on lead. We therefore undertook a range of studies of the simple situation in which films of PbO_2 were formed on pure lead and some alloys of interest: this paper records the results.

2. Experimental

PbO_2 electrodes ($\phi = 0.071$ cm^2; sheathed in Teflon) were formed in 5 M H_2SO_4 solution from lead and lead alloys by momentarily polarizing at 2000 mV to start PbO_2 formation and then continuing polarization in the PbO_2 potential region (1250 mV) until the current had fallen to an acceptably low (and constant) level. Impedance measurements were made with a frequency response analyser (Solatron 1170) controlled by microprocessor logic (Kemitron). At the reversible potential in 5 M H_2SO_4 and more positive potentials, electrodes were simply poised at the desired potential and the impedances measured in the range 10 kHz to 0.001 Hz. At potentials negative to the reversible potential impedances were measured only when the electrode reduction current had fallen to zero at the potential of interest. In this way the impedances were measured at well-defined pre-electrode states rather than at the ill-defined ones which exist if there is significant electrode reduction current. (It should be noted, however, that if potentials other than the reversible are to be investigated for kinetic data then there is no alternative to the a.c. on d.c. experiment with some uncertainty due to film formation [2, 3].)

3. Results and discussion

3.1. *Measurements at the reversible potential*

This was determined as the zero-current potential and found to be 1.100 V as the mean value over all the alloy systems investigated. Accordingly measurements were made throughout at this potential. The other approach of using a carefully determined E_r for each alloy led to second-order differences in the experimental E_r ($\sim$ 1 mV) which arose apparently from metallurgical effects. We have considered it more useful to fix the potential, as a consistent potential (versus Hg_2SO_4/Hg, 5 M H_2SO_4) is a better basis for comparison of impedance data.

Fig. 1 shows the Sluyters plot for pure lead to be a rising curve exhibiting neither a well-defined high-frequency shape nor a Warburg line indicating an interpretable solution process. The Randles plot corresponding to this behaviour is shown in Fig. 2. This consists of two diverging lines of which the resistive component line crosses that for the capacitative component. This behaviour is similar to that observed by Canagaratna *et al.* [6]. Figs. 3–9 show impedance loci corresponding to the other alloys investigated. At low frequency the behaviours are very similar and nowhere did we find an expected slope of either $\pi/4$ for a planar or $\pi/8$ for a porous electrode. We can conclude from this that the electrode reaction did not involve the free diffusion of species at the electrode. An examination of corresponding Randles plots for the cases shown (Figs. 3–9) indicates a divergence of the resistive and capacitive lines with cross-overs at high frequency. This supports an argument for the reaction occurring completely in the adsorbed state with nothing leaving the electrode. Such a mechanism would fit in with the known adsorptive properties of lead dioxide [7].

At high frequency the impedance data show considerable differences between the alloys and

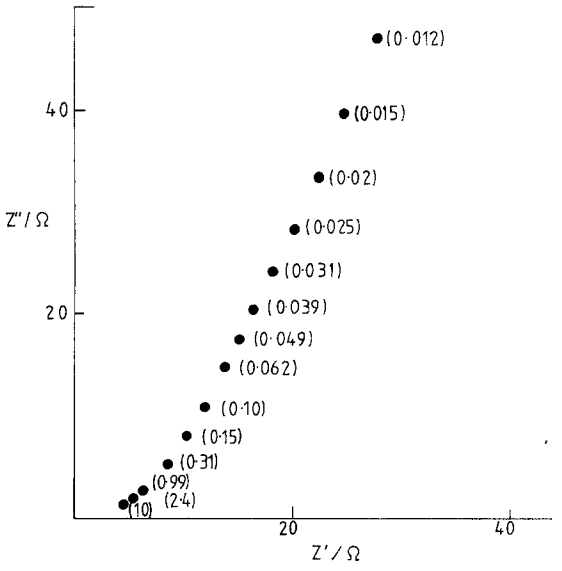

Fig. 1. The complex-plane plot (Sluyters plot) for a pure lead electrode ($\phi = 0.071$ cm^2) in 5 M H_2SO_4 at 23° C; 1100 mV; frequencies in kilohertz are given in parentheses.

unalloyed lead. The most noticeable feature occurs with lead–antimony alloy where the presence of a well-developed inductive loop at the highest frequencies is quite distinctive. None of the other alloys exhibits this, but data reported in the literature [2] for lead dioxide electrodes show that this behaviour occurs with porous lead dioxide electrodes and is confirmed for lead cells by Keddam *et al.* [8]. The occurrence of the high-frequency inductive semicircle is a consequence of the porous nature of the electrode and the consequential electrochemistry which occurs over a distributed region of the electrode. At sufficiently high frequencies the phase angle of the Faradaic impedance is negative; this arises physically because of a change in reactant concentration with depth in the porous electrode, which clearly cannot be with a plane electrode. With the antimonial lead electrode this inductive loop is perfectly developed indicating that the pores are effectively semi-infinite, i.e. about four times the characteristic diffusion length $(D/\omega)^{1/2}$ within the frequency range. This also suggests a more tightly adherent film [9] in accordance with a smaller separation between conductor and dielectric and the flat-capacitor theory.

We have shown previously [10] that additions of bismuth to calcium–tin–lead battery alloys cause an increase in the cycle life of the alloy in sulphuric acid. This is confirmed in the present investigation when Figs. 7 and 8 are compared. We observe that both the resistance and capacitance of the electrode are decreased with the addition of Bi to Pb–Ca–Sn in agreement with the formation of a layer which is rather less passivating. The outstanding observation at this potential is the lack of any well-defined shapes concerning the electrochemistry. The reason for this must lie in the slowness of the phase formation reactions and the lack of exchange due to this

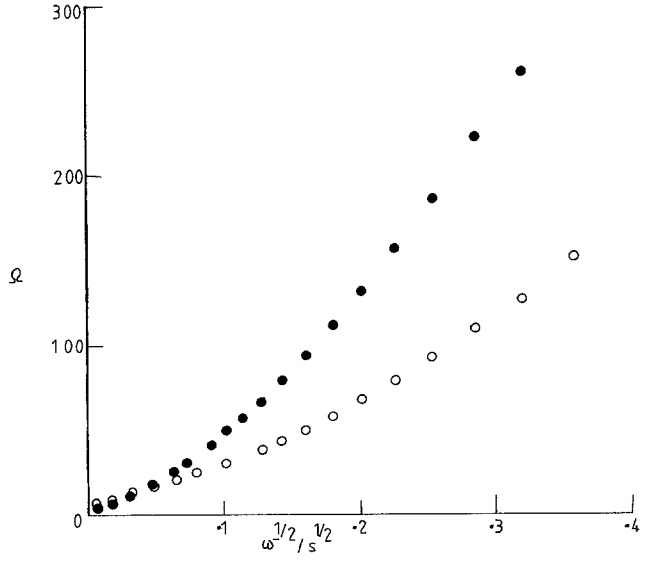

Fig. 2. The Randles plot corresponding to the system of Fig. 1 at 1100 mV. •, $1/\omega C$; ○, R.

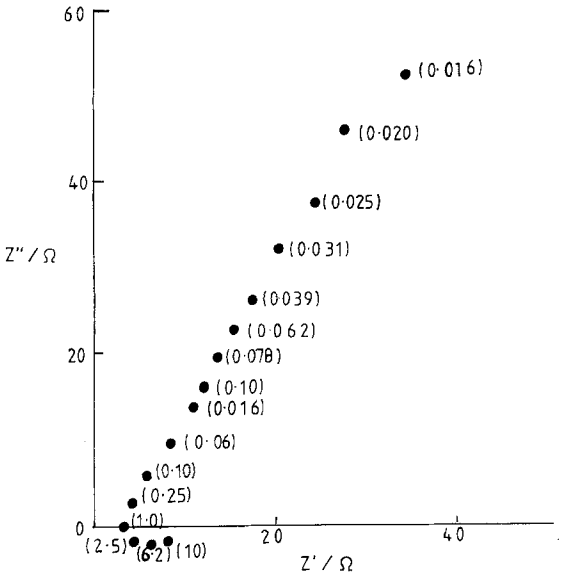

Fig. 3. Details as for Fig. 1, but for Pb–Sb (5.15%).

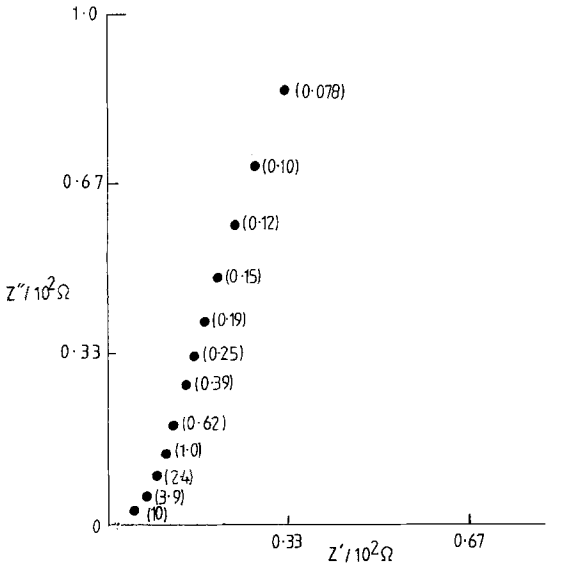

Fig. 5. Details as for Fig. 1, but for Pb–Bi (0.13%).

cause. The slope of the low-frequency part of the impedance shape is always much greater than the expected Warburg slope 45° (for a plane electrode) or 22.5° (for a porous electrode). Although there is a little evidence for curvature in this frequency region the electrode is effectively polarizable, and the change in slope may simply reflect the porosity.

The results on pure lead and the alloys not containing antimony agree quite well with the impedance shapes reported by Casson *et al.* [3] for electrodeposited β-PbO_2. We can conclude from this that in the positive region of the equilibrium the deposit on the non-antimonial lead resembles β-PbO_2; however, on the antimony alloy the formation of PbO_2 involves the formation of a pore structure sufficiently well developed to cause a high-frequency inductive shape.

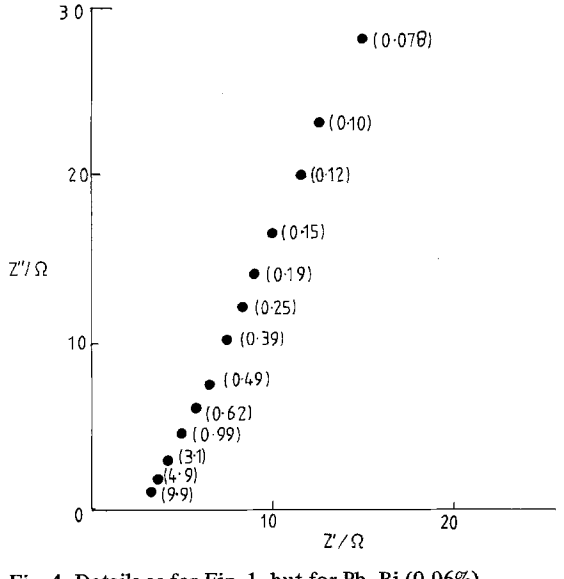

Fig. 4. Details as for Fig. 1, but for Pb–Bi (0.06%).

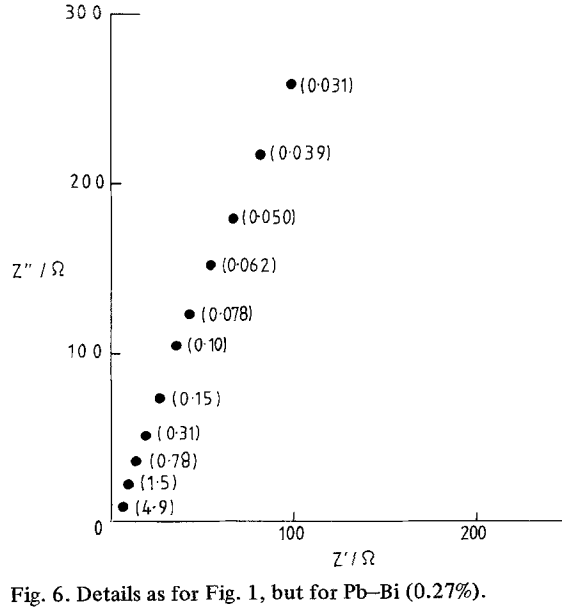

Fig. 6. Details as for Fig. 1, but for Pb–Bi (0.27%).

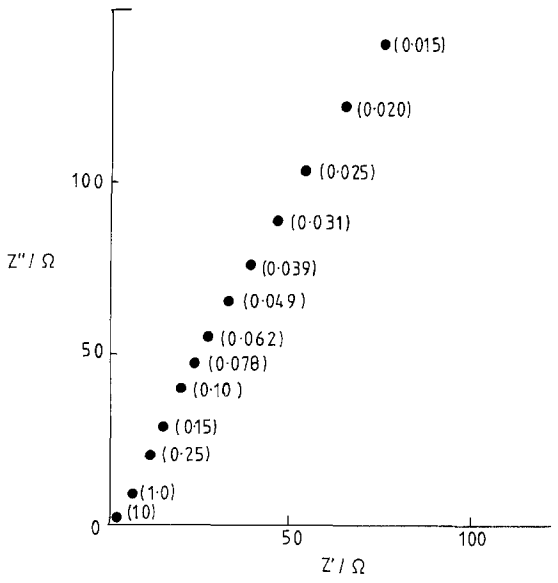

Fig. 7. Details as for Fig. 1, but for Pb–Ca–Sn.

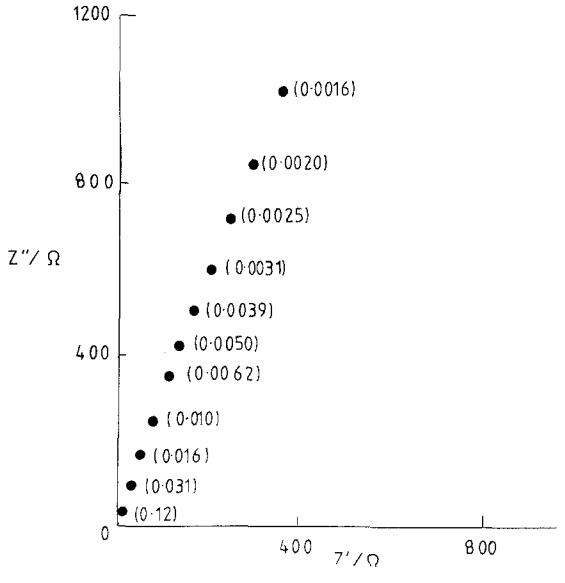

Fig. 9. Details as for Fig. 1, but for Pb–Ca–Sn–Mg (0.046%).

3.2. *Measurements at polarized electrodes*

3.2.1. Pure lead. When the electrode is forced to potentials positive to the equilibrium potential oxygen gas is produced at the electrode, the bubbles increasingly obscure the electrode and its impedance changes continuously with time. Provided that the potential is not too positive and measurements are made rapidly an 'accurate enough' impedance loci can be obtained. Such a one is shown in Fig. 10. It consists of an almost vertical straight line approximating to ideal polarizability. It is clear that there is no useful kinetic information to be gathered and it must be concluded that when the potential is sufficiently negative, so that the oxygen evolution reaction does not intrude by physical obscurance of the electrode, the reaction is so slow as to render the electrode effectively polarizable.

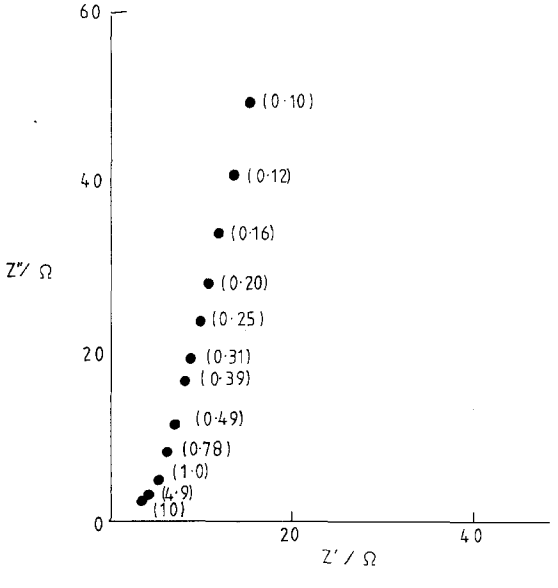

Fig. 8. Details as for Fig. 1, but for Pb–Ca–Sn–Bi (0.15%).

When the electrode potential is shifted to potentials more negative than the equilibrium in the range below 970 mV, which is the 'operational' potential of PbO_2 electrodes in battery situations, the impedance loci become that of a system rate-controlled by electron transfer. A high-frequency semicircle is apparent which goes off at lower frequency to form an inclined line. This behaviour is shown by Figs. 11–14 for a series of potentials in the range 1000–930 mV. A feature of the figures is that the dihedral angle of the low-frequency tail exceeds $\pi/4$; furthermore this angle increases as frequency is decreased. This cannot be attributed to the PbO_2 or any intermediate phase between the lead base and the PbO_2 and must therefore be attributed to the lead sulphate grown on the lead dioxide as a result of the potential excursion. Even though the current flowing across the electrode interfaces had effectively

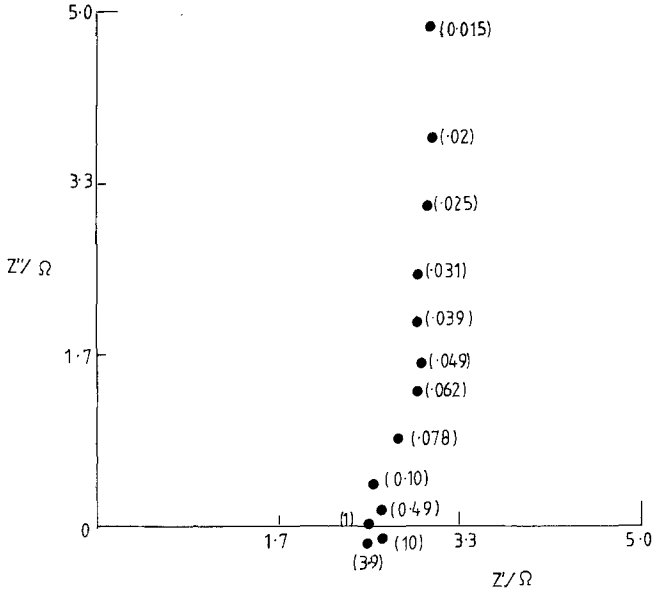

Fig. 10. Complex-plane plot for pure lead electrode potentiostatted at 1250 mV. Other details as for Fig. 1.

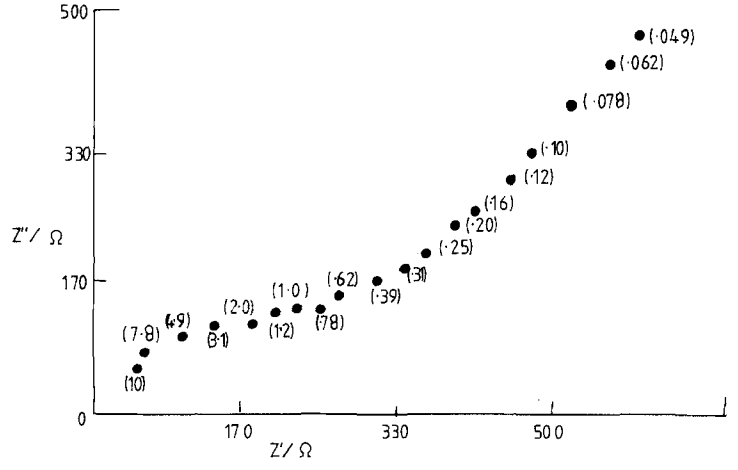

Fig. 11. Complex-plane plot for pure lead at 970 mV (for details see Fig. 1).

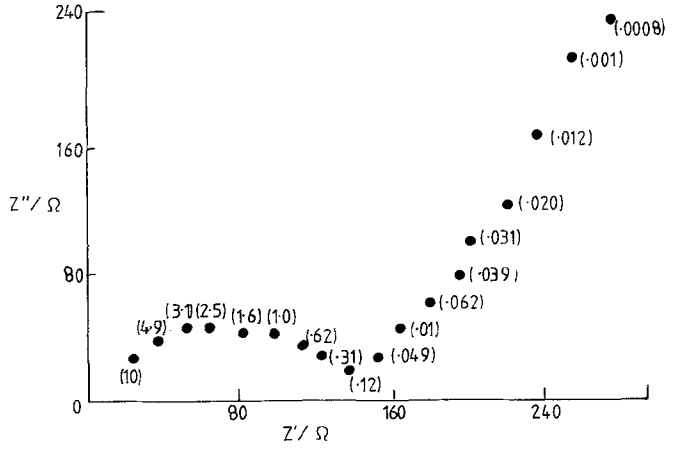

Fig. 12. Complex-plane plot for pure lead at 950 mV (for details see Fig. 1).

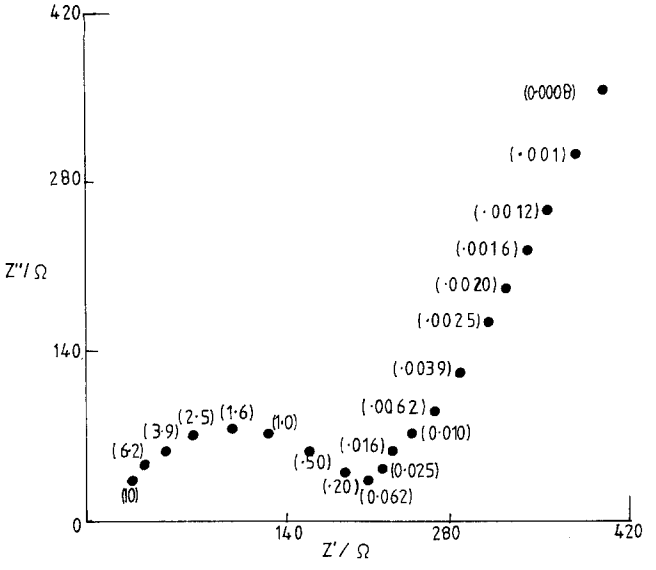

Fig. 13. Complex-plane plot for pure lead at 940 mV (for details see Fig. 1).

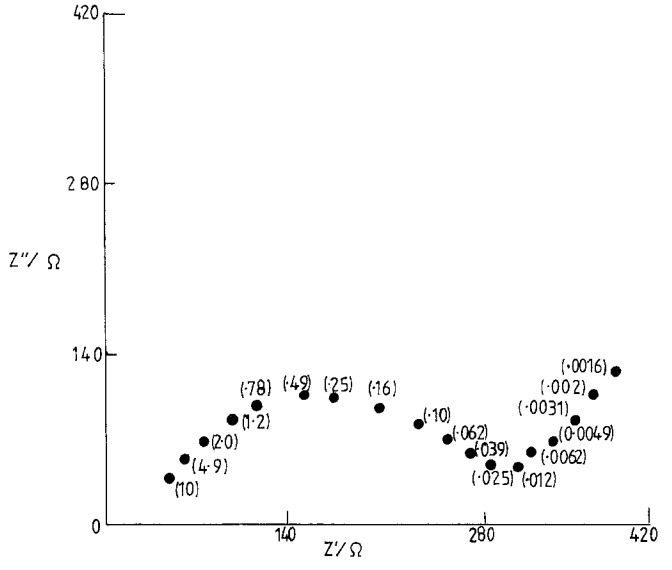

Fig. 14. Complex-plane plot for pure lead at 930 mV (for details see Fig. 1).

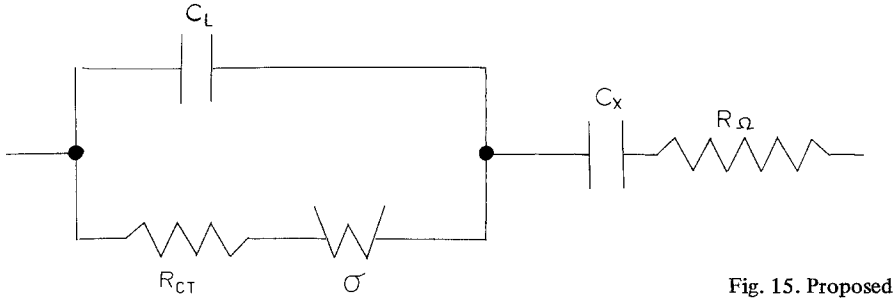

Fig. 15. Proposed model for cell analogue.

Table 1. Electrode characteristics obtained from computer match for a pure lead electrode at various potentials (ϕ = 0.071 cm²)

Potential (mV)	*950*	*940*	*930*
R_Ω (Ω)	22.17	39.38	57.59
R_{CT} (Ω)	100.2	155.9	219.3
C_L (μF)	0.721	0.630	0.602
σ (Ω s$^{-1/2}$)	449.5	414.5	514.2
C_X (μF)	1702	1820	7200

reached zero, the sulphate layers did not passivate the electrodes, rather the rate of reaction was slowed down. The electrode behaves therefore as a reaction controlled by charge transfer and diffusion in solution in series with a leaky capacitance representing the sulphate layer. This is convincingly confirmed in Fig. 16 in which the analogue shown in Fig. 15 is matched to the experimental data. The matching was carried out by writing the complex equations for the cell analogue:

$$Z_D = -i/\omega C_L \quad (1)$$

$$Z_F = R_{CT} + \sigma\omega^{-1/2} - i\sigma\omega^{-1/2} \quad (2)$$

for which the impedance is given by

$$Z' = \left(\frac{1}{Z_D} + \frac{1}{Z_F}\right)^{-1} - i/\omega C_X + R_{sol}. \quad (3)$$

Equation 3 was decomposed into the real and imaginary parts and each was treated separately by expanding about approximate values (x') of the circuit elements (x) such that

$$x = x' + \Delta x. \quad (4)$$

Using Taylor's theorem and neglecting the second- and higher-order terms, we obtain two linear equations

$$R = R' + \sum \left(\frac{dR'}{dx}\right) \Delta x \quad (5a)$$

and

$$C = C' + \sum \left(\frac{dC'}{dx}\right) \Delta C. \quad (5b)$$

In order to calculate values of R' and C' and their differentials, approximate values of x are substituted in the expressions for each of the n experimental data points. These n linear equations are reduced by the method of least squares to the C normal equations needed to calculate Δx for each circuit element. The approximate value of x is then corrected by Δx and the process is repeated until Δx is sufficiently small to be neglected.

The calculation and isolation of real and imaginary parts of Z' of the impedance were performed using complex-number handling capability of the computer (PRIME 400). Fig. 16 confirms that the behaviour, especially at low frequency, is adequately described by the model of an electrode becoming progressively blocked by a passivating layer of $PbSO_4$ as the potential is driven to more

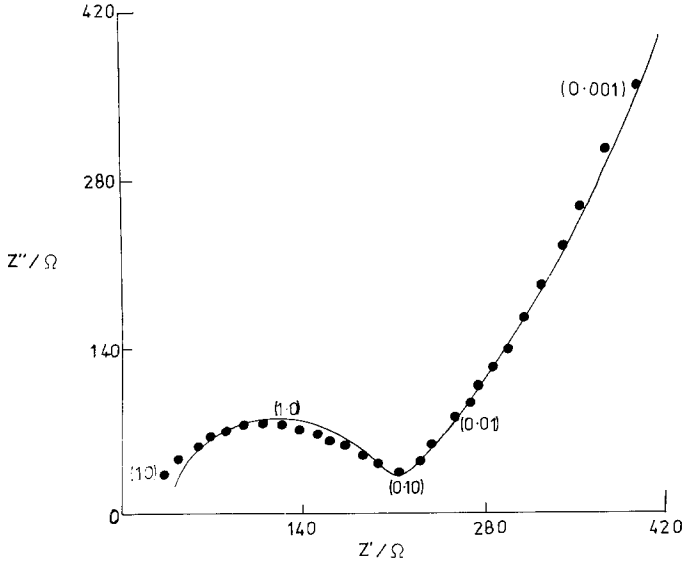

Fig. 16. Agreement between the experimental data and computer match for a pure lead electrode at 940 mV (details as in Fig. 1). The dots (•) show experimental data and the line shows the computer match.

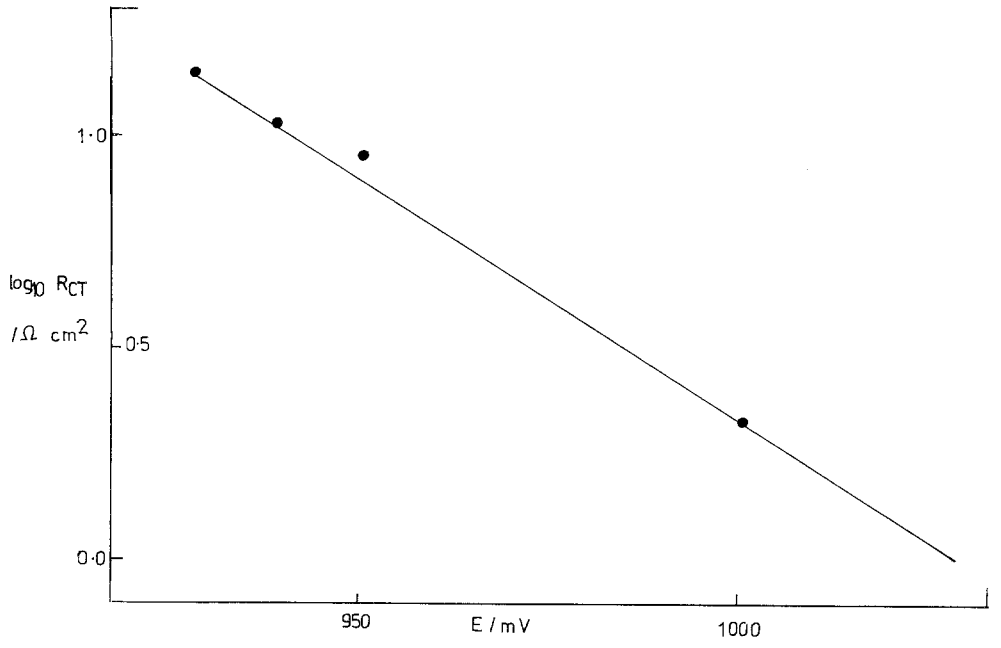

Fig. 17. Plot of $\log_{10} R_{CT}$ versus potential for a pure lead electrode in the potential region 930–1000 mV.

negative potentials. The data from the computer match is shown in Table 1. The film resistance is effectively R_Ω and this is seen to increase as more $PbSO_4$ is formed on the electrode. The film capacitance increases as potential decreases as more of the surface is covered more effectively with the dielectric. The Warburg coefficient increases with decreasing potential as the diffusing area of the electrode is reduced by the more effectively covering film.

It was not possible to obtain a well-defined correlation with potential for either R_Ω, σ, C_L or C_X; however, in the case of R_{CT} a linear relationship was found between $\log R_{CT}$ and E. This is shown in Fig. 17 in which a decade increase in R_{CT} is the result of an 84 mV decrease in potential. This value expresses both the reduction in the effective area of the electrode as a result of the increasing cover passivity and the increase in the reduction rate constant due to the change in potential. Casson *et al.* [3] found that the Tafel slope for the latter factor was − 87 mV per decade so that the passivity factor is a 43 mV per decade change in effective area, i.e. a decrease of 43 mV in potential results in a decade decrease in active surface area.

Using the model as proposed generally gives a satisfactory fit with the experimental data (Fig. 16); however, at the most negative potentials the high-frequency semicircle was noticeably flattened. This can be considered to be due to surface heterogeneity although an alternative and more likely explanation is that there is a certain amount of adsorption of reactants and products in the sense of Laitinen and Randles [11]. In the adsorbed state, the electrode reaction

$$PbO_2 + 4H^+ + SO_4^{2-} + 2e \rightleftarrows PbSO_4 + 2H_2O$$

occurs giving rise to a further circuit element which shunts the double layer and the reaction. This has been discussed by Kelly *et al.* [12]. The values of the circuit components obtained using this model are sufficiently close to the ones obtained without considering adsorption (Table 2) for our present purpose. In view of doubt about the precise reason for the high-frequency flattening we preferred to use the simpler model here.

3.2.2. Alloys of commercial significance. Figs. 18–23 show typical impedance loci of the series of alloys in the above potential range. Basically the curve is as observed for pure lead; however, the magnitudes of the circuit elements are rather different. Table 2 shows the salient data. It is clear that the effect of the alloying ingredients to the pure lead is to modify all the characteristics of the

Table 2. Electrode characteristics for various alloys at various potentials; data obtained from computer match (ϕ = 0.071 cm²)

	Pb–Sb	*Pb–Bi* (0.06%)	*Pb–Bi* (0.13%)	*Pb–Bi* (0.27%)	*Pb–Ca–Sn–Bi* (0.15%)
970 mV					
R_Ω (Ω)	32.26	2.65	11.78	30.2	9.22
R_{CT} (Ω)	22.76	32.91	45.02	113.9	28.36
C_L (μF)	0.909	0.89	0.949	0.285	0.860
σ (Ω $s^{-1/2}$)	896	741.8	354	2113	832.6
C_X (μF)	167	664	389	157	195
950 mV					
R_Ω (Ω)	38.48	9.06	17.45	113.4	41.86
R_{CT} (Ω)	38.07	71.40	105.4	396.9	190.4
C_L (μF)	0.925	0.827	0.742	0.248	0.265
σ (Ω $s^{-1/2}$)	1117	634.4	469.8	1909	4290
C_X (μF)	297	948	1350	230	74.1
940 mV					
R_Ω (Ω)	34.3	12.53	26.75	133.2	14.77
R_{CT} (Ω)	36.4	101.7	164.8	628.8	54.65
C_L (μF)	0.740	0.796	0.749	0.227	1.001
σ (Ω $s^{-1/2}$)	1296	5638	389.1	2215	652
C_X (μF)	424	1290	1720	251	681
930 mV					
R_Ω (Ω)	41.17	32.16	28.87	209.1	25.3
R_{CT} (Ω)	47.92	163.9	241.5	1161	192.2
C_L (μF)	0.78	0.783	0.733	0.214	0.742
σ (Ω $s^{-1/2}$)	1362	565.8	416.6	2992	1586
C_X (μF)	464	1430	1910	388	448

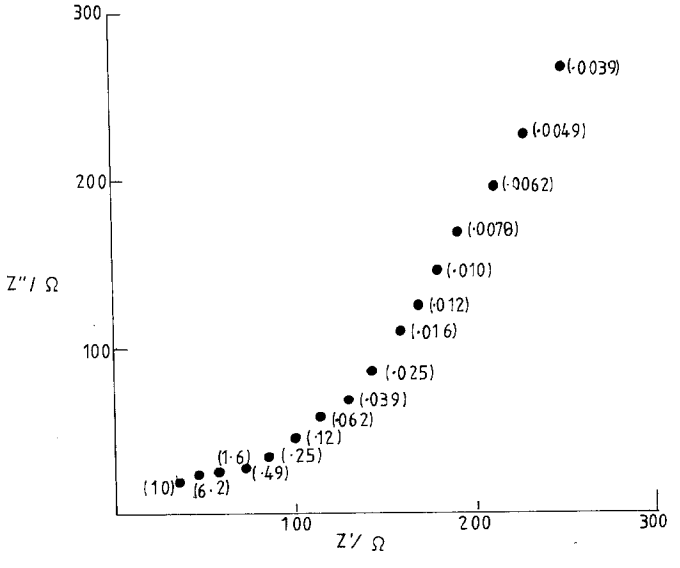

Fig. 18. Sluyters plot for Pb–Sb (ϕ = 0.071 cm²) in 5 M H_2SO_4 at 23° C; 950 mV.

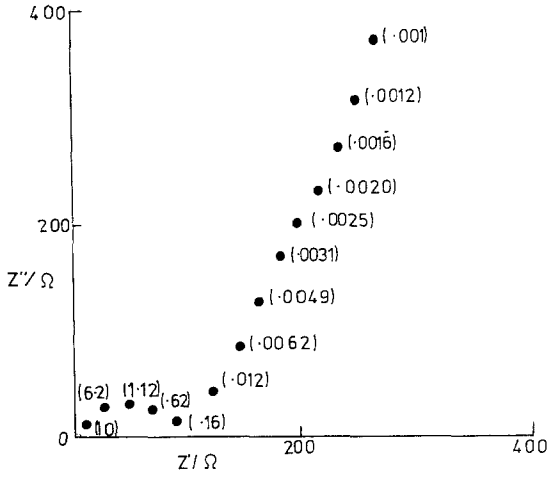

Fig. 19. Details as Fig. 18, but for Pb–Bi (0.06%).

electrode analogue (Table 2). Antimony, which may be taken as the optimum alloying ingredient for a pasted plate, has a very marked effect on all the component magnitudes. At all potentials the effective charge-transfer resistances are lower, the double-layer capacitance increased and the capacitances of the electrode sulphate layer are very much reduced, although similar values of the sulphate film resistance are observed. These observations point to a thicker electrode film produced on the antimonial lead than on the antimony-free lead. However, the values of the effective Warburg coefficients indicate an effectively larger area available for diffusion in the case of the antimony alloy. These are remarkable and interesting findings, for usually a thicker film engenders better coverage, a higher R_{CT} and a higher σ value. We must conclude from this that although the film on antimonial lead is thicker than that on pure lead it is more porous and perforated and that even though the charge-transfer reaction is able therefore to occur relatively readily diffusion is difficult resulting in a higher σ value.

Of the few alloys investigated, the alloy which produces an effect most like that of Pb–Sb is that produced by the addition of a small amount of bismuth to the Pb–Ca–Sn alloy, although the effective film resistance is considerably lower than either the lead or the antimonial lead alloy. This observation strengthens our idea that Bi in the alloy produces a resulting sulphate film which has improved conductivity, probably due to the imparting of semiconductor properties by a doping process.

We have shown in a previous paper [13] how, of the three Bi–Pb alloys investigated here, the 0.12% Bi alloy represents the best for battery behaviour. This fact is again indicated here, for, using the behaviour of the antimonial lead as the optimum, this intermediate concentration produced the most antimonial-like behaviour.

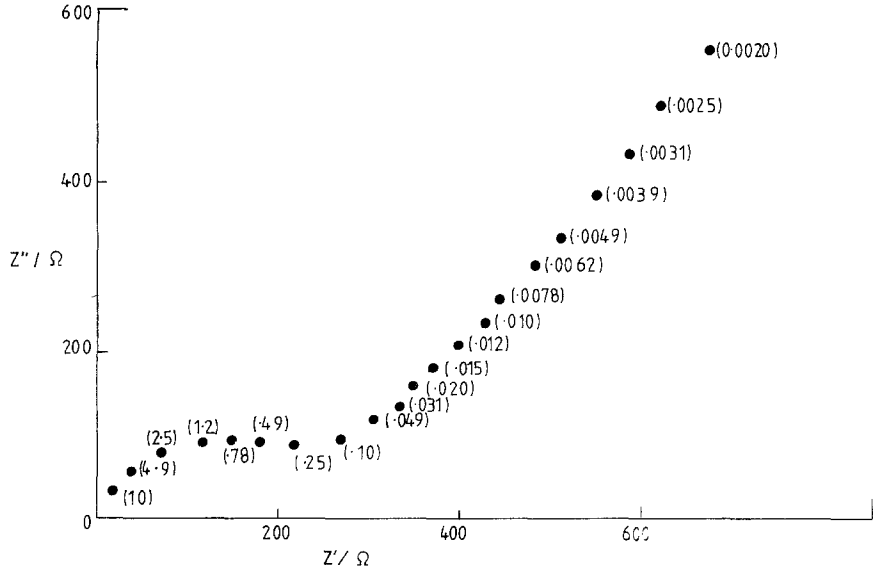

Fig. 20. Details as Fig. 18, but for Pb–Bi (0.13%).

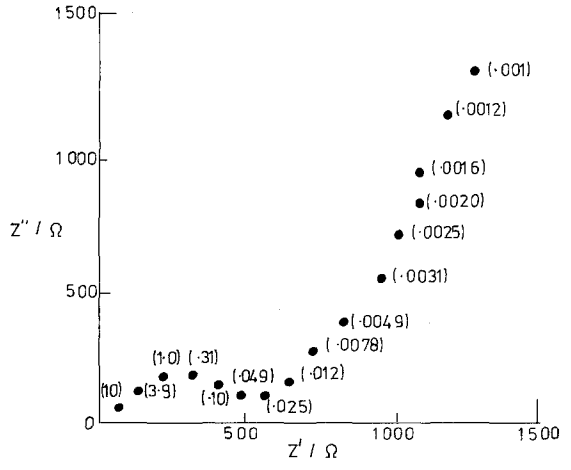

Fig. 21. Details as Fig. 18, but for Pb–Bi (0.27%).

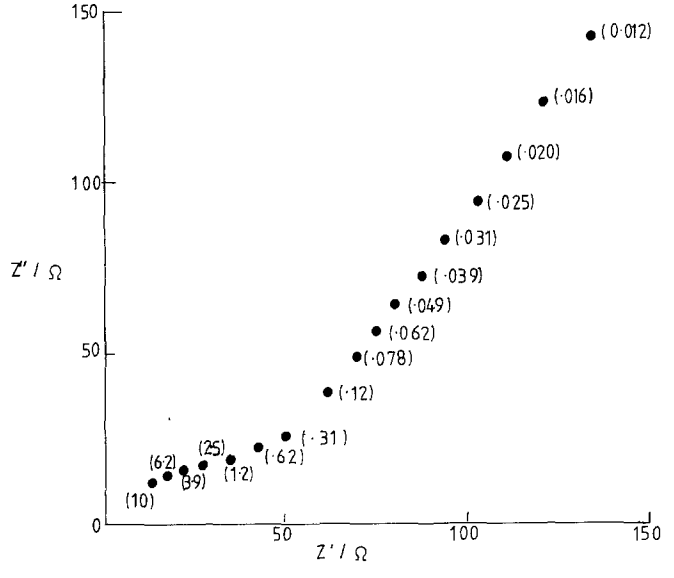

Fig. 22. Details as Fig. 18, but for Pb–Ca–Sn.

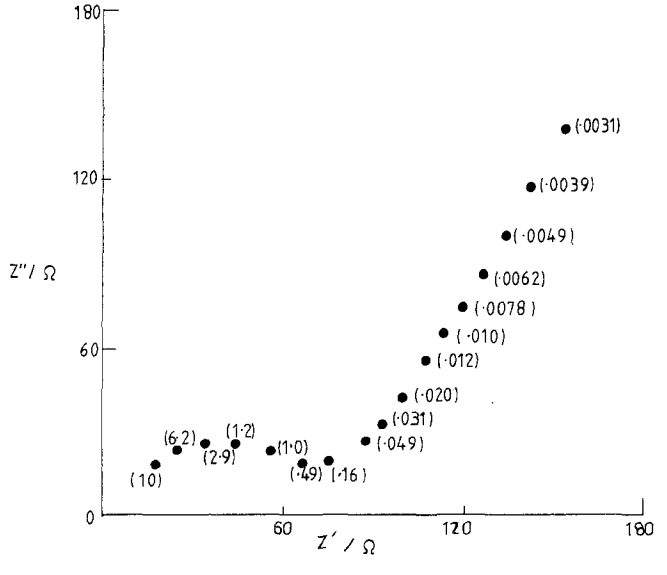

Fig. 23. Details as Fig. 18, but for Pb–Ca–Sn–Bi (0.15%).

4. Conclusions

The most important conclusions from this study are:

(a) The appearance of an inductive loop in the impedance loci of PbO_2 layers on Sb–Pb alloy (absent in the same experimental frequency range with other alloys) indicates that the effect of Sb is to produce a more porous deposit.

(b) The $PbSO_4$ film on the partially discharged electrode behaves effectively as a capacitor in series with the Faradaic path.

(c) The capacitance of the films on Sb alloy is lower than that on other alloys although it is thicker and apparently produces a more restricted diffusional path than other alloys.

(d) Bismuth appears to contribute semiconductor effects to the films developed on the product PbO_2.

References

[1] M. Sluyters-Rehbach and J. H. Sluyters, in 'Advances in Electroanalytical Chemistry, (edited by A. J. Bard) Marcel Dekker, New York (1967) Ch. 1.

[2] S. G. Canagaratna and N. A. Hampson, *Surf. Technol.* 5 (1977) 163.

[3] P. Casson, N. A. Hampson and M. J. Willars, *J. Electroanal. Chem.* 97 (1979) 21.

[4] M. Keddam, Z. Stognov and C. Lestrade, *J. Appl. Electrochem.* 7 (1977) 539.

[5] R. Darby, *J. Electrochem. Soc.* **116** (1966) 392, 496.

[6] S. G. Canagaratna and N. A. Hampson, *J. Electroanal. Chem.* 86 (1978) 361.

[7] J. P. Carr, N. A. Hampson and R. Taylor, *ibid* 27 (1970) 201.

[8] M. Keddam, S. Stymar and H. Takenoute, *J. Appl. Electrochem.* 7 (1977) 539.

[9] M. A. Dasoyan and I. A. Aguf, in 'Current Theory of Lead Acid Batteries', Technicopy Ltd, Gloucester, England (1979). Ch. 3.

[10] S. Kelly and N. A. Hampson, *1980 Brighton Power Sources Symposium,* in 'Power Sources 8', (edited by J. Thompson) Academic Press, London (1981).

[11] H. A. Laitinen and J. E. B. Randles, *Trans. Faraday Soc.* **51** (1955) 54.

[12] S. Kelly, N. A. Hampson, S. A. G. R. Karanathilaka and R. Leek, *Surf. Technol.* (1981).

[13] N. A. Hampson, S. Kelly and K. Peters, *J. Electrochem. Soc.* **127** (1980) 1456.